Fracture Investigation of the Ductile Materials Using Phase-Field Model

Peyman Esmailzadeh[1], Mohsen Agha Mohammad Pour[1], Reza Abdi Behnagh[2], and Dong Lin[3]

[1]Urmia University of Technology
[2]Affiliation not available
[3]Kansas State University

May 18, 2020

Abstract

Phase-field models have been the subject of a great deal of research in recent years. Investigations have revealed that the phase-field model is capable of generating complex crack patterns. This is gained by replacing the sharp discontinuities with a scalar phase damage field comprising the diffuse crack topology. In the previous models, cracks are blurred into the surrounding areas due to introducing dependency of degradation function to a single parameter, strain threshold. The stable crack initiation and propagation require estimation of complex higher-order degradation function, which should be solved either by a new iteration scheme or using extremely small loading increment. However, this demands considerably high computational cost. In this study, the nonlinear coupled system comprising the linear momentum equation and the diffusion-type equation governing the phase-field evolution is solved concurrently through a Newton–Raphson approach. Moreover, an improved degradation function and staggered iteration scheme are solved by a one-step paradigm is proposed. Such that the computational costs can be reduced, and the stability of crack propagation can be improved. A phase-field model for ductile fracture is carried out in the commercial finite element software Abaqus by means of UEL and UMAT subroutines. Post-processing of simulation results is implemented through an added subroutine implemented in the visualization module. Several benchmark problems show the proposed model's ability to reproduce some essential phenomenological characteristics of ductile fracture as documented in the experimental literature.

Fracture Investigation of the Ductile Materials Using Phase-Field Model

Peyman Esmaeilzadeh[1], Mohsen Agha Mohammad Pour[1], Reza Abdi Behnagh[1*], Dong Lin[2]

[1]Faculty of Mechanical Engineering, Urmia University of Technology, Urmia, Iran

[2]Department of Industrial and Manufacturing Systems Engineering, Kansas State University, USA

[*]**Corresponding author** : r.abdibehnagh@uut.ac.ir

Abstract

Phase-field models have been the subject of a great deal of research in recent years. Investigations have revealed that the phase-field model is capable of generating complex crack patterns. This is gained by replacing the sharp discontinuities with a scalar phase damage field comprising the diffuse crack topology. In the previous models, cracks are blurred into the surrounding areas due to introducing dependency of degradation function to a single parameter, strain threshold. The stable crack initiation and propagation require estimation of complex higher-order degradation function, which should be solved either by a new iteration scheme or using extremely small loading increment. However, this demands considerably high

computational cost. In this study, the nonlinear coupled system comprising the linear momentum equation and the diffusion-type equation governing the phase-field evolution is solved concurrently through a Newton–Raphson approach. Moreover, an improved degradation function and staggered iteration scheme are solved by a one-step paradigm is proposed. Such that the computational costs can be reduced, and the stability of crack propagation can be improved. A phase-field model for ductile fracture is carried out in the commercial finite element software Abaqus by means of UEL and UMAT subroutines. Post-processing of simulation results is implemented through an added subroutine implemented in the visualization module. Several benchmark problems show the proposed model's ability to reproduce some essential phenomenological characteristics of ductile fracture as documented in the experimental literature.

Keywords:

Finite element analysis, Ductile fracture, Crack propagation modeling, Crack path; Fracture mechanics

Symbol	**Name**
$\mathbb{B}_I^{\mathbf{u}}$	Strain-displacement Tensor
$\mathbb{B}_I^{\varphi}$	Strain-Phase field Tensor
$E_{\updownarrow}$	Total energy
$\mathbf{F}^{\mathbf{u}}_{\mathrm{I\,ext}}$	External force
$\mathbf{F}^{\mathbf{u}}_{\mathrm{I\,int}}$	Internal force
g_p	Plastic phase field function
H_e	History variable
h	Hardening modulus
$\mathbb{K}$	Stiffness matrix
$\updownarrow$	Length scale
N_I^u	Displacement shape function
N_I^{φ}	Phase field shape function
n	Calibration parameter
p	Accumulated plastic strains
q	Calibration parameter(Stabilization)
$\mathbf{r}_I^{\mathbf{u}}$	Displacement field Residual
$\mathbf{r}_I^{\varphi}$	Phase field Residual
$\mathbf{u}$	Displacement field
α	Internal hardening variable
ε	Strain
$\varepsilon^p_{\mathrm{eq,crit}}$	Critical plastic strain
$\varepsilon^p_{\mathrm{eq}}$	Equivalent plastic strain
Γ	crack set
η	Stabilization parameter
$\mu,\ \lambda$	Lame constants
$g\,(\varphi)$	Phase field function
$g\,(\varphi,p)$	Plasticity dependent phase field function
φ	Phase-Field parameter
φ_c	Maximum value of damage
ψ^e	Total elastic energy
ψ_p	Plastic energy
${\psi_e}^+$	Elastic energy(tension)
${\psi_e}^-$	Elastic energy(compression)
Ω	Reference configuration
$\mathcal{G}_c$	Fracture toughness

Introduction

Identification of failure mechanisms and the development of computational methods that precisely estimate complex failure and fracture mechanisms in ductile materials has proven difficult, and many strategies with varying success have been suggested. The phase-field method, also known as the variational approach to fracture, is an approach that has continually been the topic of both scientific interest and paramount importance in engineering applications, which has challenging mathematical and numerical implications.

However, the provision of computational predictive equipment allows for significant financial savings of the cost of experiments, mainly in instances wherein those are extremely complicated, as well as for design optimization.

Following the comprehension review in previous works[1], several modeling approaches have been proposed for ductile fracture. For brittle and ductile materials, the basic idea is typically primarily based on the thermodynamic framework first delivered via Griffith.[2] The propagation of pre-existing cracks in the phase-field model agrees with the energetic considerations of classical Griffith theory.[3,4] The variational approach to brittle fracture, developed by Francfort and Marigo[5], to find a solution to the fracture-using minimizing potential energy-based totally on Griffith's concept of brittle fracture. This method results in Mumford-Shah[6]. Bourdin *et al* [7] approved straightforward numerical solutions. An alternative formulation, based on continuum mechanics and thermodynamic theories, become provided by means of Miehe[8] and Miehe *et al* .[9]

Besides an alternative derivation, Miehe *et al* [8]introduced a crucial mechanism for distinguishing tensile and compressive results on crack growth. The works of Larsen[10], Larsen *et al* [11], Bourdin *et al* [12], Borden *et al* [13], and Hofacker and Miehe[14]demonstrate that this technique can be applied to dynamic fracture and produces results that are consistent with considerable benchmark challenges. Preliminary work to extend the variational approach to ductile materials has been stated in Ambati *et al* [14,15] and Miehe *et al* [17,18].They examined the degradation function as a function of the accumulated plastic strain including the elastic modulus, the yield stress, and the strain hardening exponent. The coupled set of stress equilibrium equations and the phase-field evolution are solved at the same time in the work of Miehe and Welschinger[9]. A staggered scheme is being used in the work of Miehe *et al* [8] and Aldakheel[17]. Wherein a local energy history field,H, is adopted as a state variable to guarantee irreversible crack growth.

A related approach is introduced by McAuliffe and Waisman[19] where a model that couples the phase-field with the ductile shear band is improved. On this technique, shear bands are formulated the usage of an elastic-perfectly viscoplastic model and fracture is modeled as the degradation of the volumetric elastic stress terms only.

Ductile fracture of elastic-plastic solids turned into an investigation underneath dynamic loading conditions. In the works of Miehe[20,21] the point of interest turns out to be placed on reproducing the experimentally determined ductile to brittle failure mode with an increased loading pace. In these works, the whole (free) energy functional is taken because of the accumulation of elastic, plastic and fracture contributions. Recently, Duda *et al* [22] introduced a phase-field model for quasi-static brittle fracture in elastoplastic solids. T. Gerasimov *et al* [23] proved that the irreversibility constraint of the crack phase-field is a constrained minimization problem. Bhattacharya *et al* [24] presented variational gradient damage formulation of ductile failure that naturally couples elasticity, perfect plasticity, and fracture in the rate-independent setting. In this work, small plastic deformation is considered to take place in the location of the notch root or crack tip. Also, in this case, the governing equations in terms of general energy are the sum of elastic, plastic and fracture contributions. The elastic and fracture contributions take the classical form, while the plastic contribution is a delegated function of the accumulated plastic strain.

The objective of this paper is to propose a phase-field formulation of ductile fracture in elastoplastic solids, in the quasistatic boundary problems of linear elastoplasticity with a linear isotropic hardening material. A coupling between the degradation function introduced in[15] is investigated. This coupling is shown to play a fundamental role in the correct prediction of some phenomenological aspects of ductile fracture evidenced from available experimental results. Moreover, the model proved to be thermodynamically consistent in [15].

One of the significant improvements of the degradation function in this work is $q \in (0, 1]$ parameter which plays a dominating role in the stability of crack propagation.

The development of computer coding via UEL and UMAT subroutines is considered. Analysis of the model yields the definition of an effective fracture strength for one element in the two-dimensional phase-field model. In the second step, the problem of crack initiation and propagation in the one element is extended in the two-dimensional setting. Therefore, based on the findings from the one element case, crack paths and force-displacement curves are derived for the proposed model.

2. Governing Equations

2.1 phase-field summary of brittle fracture of elastic solids:

The phase-field model's description of brittle fracture drives from the variational formulation of brittle fracture by Francfort and Marigo[5], and the regularized formulation of Bourdin*et al* [7]. In Bourdin's regularized model, the total energy, $E_{\updownarrow}$, of a linear elastic media is:

$$E_{\updownarrow}(\mathbf{u}, \Gamma) = \int_{\Omega} \psi^{e}(\varepsilon(\mathbf{u}))\, d\mathbf{x} + \mathcal{G}_{c} \int_{\Gamma} ds \ , \tag{1}$$

Eq.(1) and $\mathcal{G}_c$ referes to the Griffith functional and material fracture toughness, respectively. The Ω is the reference configuration of the body. The undetermined displacements,$\mathbf{u}$, as well as the crack set, Γ, can be achieved through a global minimization of such functional function under the condition of irreversibility, [25]

$$\Gamma_{t+t} \supseteq \Gamma_{t} \ , \tag{2}$$

In the Eq. (1) ψ^e is the elastic energy density function characterized as:

$$\psi^{e} = \frac{1}{2}\varepsilon(\mathbf{u}) : \mathbb{C} : \varepsilon(\mathbf{u}) \ , \tag{3}$$

where $\mathbb{C}$ is the fourth-order elasticity tensor. The infinitesimal strain tensor $\varepsilon(\mathbf{u})$ is associated with the displacement field $\mathbf{u}$ by:

$$\varepsilon(\mathbf{u}) = \frac{1}{2}\left(\nabla\mathbf{u} + (\nabla\mathbf{u})^{T}\right) \ , \tag{4}$$

The second term of Eq. (1) is a volumetric approximation of the energy contribution-the crack density functional-which typically takes the form,

$$\mathcal{G}_{c} \int_{\Gamma} ds = \mathcal{G}_{c} \int_{\Omega} \left(\frac{(1-\varphi)^{2}}{4\updownarrow} + \updownarrow |\nabla\varphi|^{2}\right) d\mathbf{x} \ , \tag{5}$$

To facilitate the numerical solution of this problem, Bourdin *et al* [26] introduced a phase-field approximation of Eq.(1) that takes the form:

$$E_{\updownarrow}(\mathbf{u},\varphi) = \int_{\Omega} \{g(\varphi)\, \psi^{e}(\varepsilon(\mathbf{u}))\}\, d\mathbf{x} + \mathcal{G}_{c} \int_{\Omega} \left(\frac{(1-\varphi)^{2}}{4\updownarrow} + \updownarrow |\nabla\varphi|^{2}\right) d\mathbf{x} \ , \tag{6}$$

The scaler value, φ, which implies the crack phase-field parameter and alters slightly from 0 (completely intact state) to 1 (fully broken). The fracture behavior of phase-field fracture models is mainly adjusted

by two parameters. The cracking resistance$\mathcal{G}_c$ is a material parameter, which is a measure for the surface or fracture energy, needed to create new fracture surfaces. The second parameter is a length scale, which primarily controls the width of the transition zone between broken and undamaged material.

The stress degradation function,$g : [0,1] \rightarrow [0,1]$performs a key role in the formulation because it regulates how the stress reacts to alterations in the phase-field. A basic quadratic degradation function, which is prevalent in literature is,[27]

$$7 \quad g(\varphi) = \varphi^2 + \eta \ ,$$

The small dimensionless parameter η models an artificial residual stiffness of a totally broken phase, $\varphi = 1$, and is essentially needed to prevent numerical difficulties. For numerical reasons (stability) η may not be chosen too small. However, too large values for η overestimate the bulk energy in fractured zones.

By applying variational principles, the minimization problem, Eq.(6) can be reformulated as the system of the stress equilibrium equation, div$\sigma(\mathbf{u}, \varphi) = 0$.

The second-order Cauchy stress tensor, σ,

$$8 \quad \sigma(\mathbf{u},\varphi) = g(\varphi) \frac{\partial \psi_e(\varepsilon)}{\partial \varepsilon} = g(\varphi)\, \mathbb{C} : \varepsilon \ ,$$

and the evolution equation for φ:

$$9 \quad 2\updownarrow\varphi + \frac{1-\varphi}{2\updownarrow} = \frac{\acute{g}(\varphi)}{\mathcal{G}_c} \ ,$$

Fundamental differences between fracture behavior in tension and compression should be taken into account. However, Eq.(3) does not differentiate between that behavior. Already in Amor *et al* [28] examples of unrealistic crack patterns under compression have been documented. To prevent such situations a derived regularized formulation of Eq.(1) has been suggested in Miehe *et al* [8,9]. The corresponding approximation takes the form as follows:

$$10 \quad E_{\updownarrow}(\mathbf{u},\varphi) = \int_\Omega \left\{ g(\varphi)\, {\psi_e}^+(\varepsilon) + {\psi_e}^-(\varepsilon) \right\} d\mathbf{x} + \mathcal{G}_c \int_\Omega \left[\frac{(1-\varphi)^2}{4\updownarrow} + \updownarrow |\nabla\varphi|^2 \right] d\mathbf{x} \ ,$$

using a specific additive decomposition$\psi_e = {\psi_e}^+ + {\psi_e}^-$of the elastic energy density ψ_e, in contrast to Eq.(6), the degradation of only the positive energy part is allowed herein, whereas the negative part remains undegraded. The ${\psi_e}^+$ represents tensile contributions and ${\psi_e}^-$ represents compressive contributions to the stored elastic strain energy. This modification provides a mechanism for distinguishing states of strain under which cracks will growth. In Contrafatto[29] the trace of the elastic strain tensor was used as separating interface. This approach has also been followed by Faria[30] and Ambati[31]. In such a way the elastic energy takes different forms according to the sign of the elastic strain tensor.[28]

$$11 \quad {\psi_e}^+(\varepsilon) = \tfrac{1}{2} k_n \langle \mathrm{tr}(\varepsilon) \rangle^2_+ + \mu \left(\varepsilon_{\mathrm{dev}} : \varepsilon_{\mathrm{dev}} \right) \ ,$$

$$12 \quad {\psi_e}^-(\varepsilon) = \tfrac{1}{2} k_n \langle \mathrm{tr}(\varepsilon) \rangle^2_- \ ,$$

Where $k_n = \lambda + 2\frac{\mu}{n}$,$\langle a \rangle_\pm = \frac{1}{2}(a \pm |a|)and\varepsilon_{\mathrm{dev}} = \varepsilon - \frac{\mathbf{1}}{\mathbf{3}} \mathrm{tr}(\varepsilon) \mathbf{I}$as well as the split based on the spectral decomposition of the strain tensor$\varepsilon = \sum_{I=1}^{3} \langle \varepsilon_I \rangle\, \mathbf{n}_I \bigotimes \mathbf{n}_I$, where $\{\varepsilon_I\}_{I=1}^3$ and$\{\mathbf{n}_I\}_{I=1}^3$ are the principal

strains and principal strain directions, respectively[8,9]. In this case, $\varepsilon_{\pm} = \sum_{I=1}^{3} \langle \varepsilon_I \rangle_{\pm} \mathbf{n}_I \bigotimes \mathbf{n}_I$and, eventually,

$$\underline{13 \quad {\psi_e}^{\pm} = \tfrac{1}{2}\lambda \langle \mathrm{tr}(\varepsilon) \rangle_{\pm}{}^{2} + \mu \mathrm{tr}(\varepsilon_{\pm})^{2} \ ,}$$

with postulate the elastic stress-strain relation, the evolution equation of the crack phase-field reading as:

$$\underline{14 \quad \sigma\left(\mathbf{u},\varphi\right) = g\left(\varphi\right) \tfrac{\partial {\psi_e}^{+}}{\partial \varepsilon} + \tfrac{\partial {\psi_e}^{-}}{\partial \varepsilon} \ ,}$$

And

$$\underline{2\updownarrow\varphi + \tfrac{1-\varphi}{2\updownarrow} = \tfrac{\acute{g}(\varphi)}{\mathcal{G}_c} {\psi_e}^{+}\left(\varepsilon\right) \ ,}$$

respectively.

To enhance the efficiency of phase-field computations, the higher-order and hybrid formulations were recommended in Miehe[8]and Ambati[32], respectively. Extension of the quasi-static formulations Eq.(5) and Eq.(9) to the dynamic setting has been presented in numerous contributions.[12,13,33,34]

2.2 Phase-field model of ductile fracture:

For the energy functional presented in Eq. (1) crack growth is driven by elastic strain energy. To extend this theory to ductile materials and provide a mechanism for plastic yielding to contribute to crack growth plastic energy density function will add,$\psi_p\left(\alpha\right)$, to the stored energy. The stored energy functional proposed in Ambati[35] is,

$$\underline{E_{\updownarrow}\left(\varepsilon^e,\varepsilon^p,\alpha\right) = \int_{\Omega} \left[\psi_e\left(\varepsilon^e\right) + \psi_p\left(\alpha\right)\right] d\mathbf{x} \ ,}$$

and

$$\underline{17 \quad \psi_p\left(\alpha\right) = \sigma_y \alpha + \tfrac{1}{2} h \alpha^2 \ ,}$$

where α is internal hardening variable, σ_y yield stress and $h > 0$ hardening modulus. In Eq. (13),ε^e and ε^p are respectively the elastic and the plastic strain tensors, which are assumed to additively contribute to the total strain,$\varepsilon = \varepsilon^e + \varepsilon^p$. The plastic strain,$\varepsilon^p$, and the hardening variable, α, take the internal (state) variables form.[36]

The free energy functional formulation suggested therein lean on the,[22]

$$\underline{18 \quad E_{\updownarrow}\left(\varepsilon^e,\varepsilon^p,\alpha,\varphi\right) = \int_{\Omega} \left\{g\left(\varphi\right) {\psi_e}^{+}\left(\varepsilon^e\right) + {\psi_e}^{-}\left(\varepsilon^p\right) + \psi_p\left(\alpha\right)\right\} d\mathbf{x} + \mathcal{G}_c \int_{\Omega} \left[\tfrac{\left(1-\varphi\right)^2}{4\updownarrow} + \updownarrow \left|\nabla\varphi\right|^2\right] d\mathbf{x} \ ,}$$

As might have known, the fracture mechanism (i.e. the evolution of the phase-field) in the brittle fracture framework is carried out mainly by the elastic strains, thus the contribution of the plastic strains will be negligible.

From the above statement, it becomes clear that a basis of the ductile phase-field model evolution is the right choice of the degradation function and, particularly, that this function should rely not only on the phase-field variable φ but also to some extent of the plastic strain state.

2.3 The proposed model

In this contribution, the recommended free energy functional is,

$$E_{\updownarrow}\left(\varepsilon^{e},\varepsilon^{p},\alpha,\varphi\right)=\int_{\Omega}\left\{g\left(\varphi,p\right)\psi_{e}{}^{+}\left(\varepsilon^{e}\right)+\psi_{e}{}^{-}\left(\varepsilon^{e}\right)+\psi_{p}\left(\alpha\right)\right\}d\mathbf{x}+\mathcal{G}_{c}\int_{\Omega}\left[\frac{(1-\varphi)^{2}}{4\updownarrow}+\updownarrow\left|\nabla\varphi\right|^{2}\right]d\mathbf{x}\ ,$$

Where the degradation function for elastic-plastic contribution can be defined as:

$$g\left(\varphi,p\right)=\left(1-\mathrm{q}\right)^{\mathrm{np}}+\eta\ , \tag{20}$$

With

$$p=\frac{\varepsilon_{\mathrm{eq}}^{p}}{\varepsilon_{\mathrm{eq,crit}}^{p}}\ ,\ \varepsilon_{\mathrm{eq}}^{p}\left(t\right)=\sqrt{\frac{2}{3}}\int_{0}^{t}\sqrt{\dot{\varepsilon}^{p}:\dot{\varepsilon}^{p}}\delta\tau\ ,$$

and $\varepsilon_{\mathrm{eq,crit}}^{p}$ as a threshold value. $\varepsilon_{\mathrm{eq}}^{p}$ is often called von Mises equivalent plastic strain. The variable p represents the accumulation and localization of plastic strains. By making dependency on φ, p and degradation function g, the fracture process will be the natural consequence of ductile damage accumulation.

The variational derivative of $E_{\updownarrow}$ with respect toε^{e} bring into the equilibrium equationdiv $\sigma\ =\ \mathbf{0}$, where the stress takes the form

$$\sigma\left(\mathbf{u},\varphi,p\right)=g\left(\varphi,p\right)\frac{\partial\psi_{e}{}^{+}(\varepsilon^{e})}{\partial\varepsilon^{e}}+\frac{\partial\psi_{e}{}^{-}(\varepsilon^{e})}{\partial\varepsilon^{e}}\ , \tag{22}$$

For the current formulation, the material complies J_2-plasticity with linear isotropic hardening, thus the Mises criterion isotropic hardening during plastic loading may be written as:

$$f\left(\sigma,\alpha,\varphi,p\right)=\sqrt{3J_{2}}\sigma_{n+1}^{\mathrm{tr}}+t_{\alpha}\leq0, \tag{23}$$

where $J_2(\sigma_{\mathrm{dev}})$ is the second principal invariant of the stress deviator tensor$\sigma_{\mathrm{dev}}=\sigma-\frac{1}{3}\mathrm{tr}(\sigma)I$ andt_{α} are the hardening thermodynamically force acquired from Eq.(16) and Eq.(14)

$$t_{\alpha}=-\frac{\partial E_{\updownarrow}}{\partial\alpha}=-(\sigma_{y}+\eta\alpha), \tag{24}$$

By using the associated flow rule this equivalent plastic strain can be shown to be equal to the plastic multiplier

$$\dot{\varepsilon}^{p}\left(\alpha,\varphi,p\right)=\dot{\lambda}\frac{\partial f}{\partial\sigma}\ ,\ \dot{\alpha}=\dot{\lambda}\frac{\partial f}{\partial t_{\alpha}}\ , \tag{25}$$

where $\dot{\lambda}$ is the plastic consistency factor. Note that these evolution equations are the same as classical J2-plasticity, where they automatically ensure the satisfaction of the second law of thermodynamics. Loading and unloading conditions are governed by the Kuhn–Tucker relations.

$$\dot{\lambda}\geq0,\ f\leq0,\ \dot{\lambda}f=0\ , \tag{26}$$

The evolution equation for the crack phase-field can be defined as

$$27 \quad 2\updownarrow\varphi + \frac{1-\varphi}{2\updownarrow} = \frac{g_{,\varphi}(\varphi,p)}{\mathcal{G}_c}{\psi_e}^{+}(\varepsilon^{\mathbf{e}}).$$

Development of the irreversibility condition, Eq.(3), to the regularized case is not instantly clear since the intermediate states$0 \leq \varphi \leq 1$ do not have a forthright physical understanding.

The natural course from the perspective of damage mechanics is to enforce the condition:

$$28 \quad \varphi(x)_{t+t} \geq \varphi(x)_t \ ,$$

this can be ordered along with an additional penalty term in the phase-field evolution equation[7], or alternatively via a history variable H which ensures the irreversibility condition to prevent crack healing. This variable, H, replaces the quantityψ_e in Eq.(27).[37]

$$29 \quad H_e(x,t) = \max \ {\psi_e}^{+}(\varepsilon^{\mathbf{e}}(x,\tau)) \ ,$$

A closer look at the phase-field localization process, however, reveals that Eq.(28) may not be the best extension of Eq. (2). Based on the observed behavior of the 1D case in Sargado[25], a strict imposition of Eq.(27) may lead to an overestimate of the crack length. Consequently, one can use a modified version of Eq.(29) in which irreversibility is imposed only when φ exceeds a certain threshold, i.e.

$$30 \quad H_e(x,t) = \begin{cases} \max \ {\psi_e}^{+}(\varepsilon^{e}(x,\tau)) & \text{if } \varphi \geq \varphi_c \\ {\psi_e}^{+}(\varepsilon^{e}(x,\tau)) & \text{otherwise} \end{cases}$$

The parameter φ_c shows the maximum value of damage that is allowed to heal during unloading. For a material point which goes through the damage $\varphi \geq \varphi_c$ the resulting stress-strain curves will be nonlinear, with the amount of departure from linearity dependent on the specific form of the degradation function.

3. Numerical solution

This section is applied to the two-dimensional implementation, which is performed under plane strain conditions in a finite element code within the Abaqus by means of UEL and UMAT subroutines. The purpose of this section is to introduce a straightforward implementation procedure. The eight-node quadrilateral finite elements are used.

Finite element approximation

In more compact form, the displacement field and phase-field are visualized inside an eight-node quadrilateral element by the following relations:

$$31 \quad \mathbf{u} = \sum_{I=1}^{m} N_I^u \mathbf{u}_I \ , \qquad \varphi = \sum_{I=1}^{m} N_I^{\varphi} \varphi_I$$

In which

$$32 \quad N_I^u = \begin{bmatrix} N_I & amp; 0 \\ 0 & amp; N_I \end{bmatrix}$$

where the subscriptions within the arrays indicate node numbers, andN_I express the element vector-field shape function correlated with node I. $\mathbf{u}_I$ and φ_I are the displacement and phase-field values at node I, respectively. In this work the standard 8-node quadrilateral element employed. So, $m = 8$. The corresponding derivative quantities are given by

$$\varepsilon = \sum_{I=1}^{m} \mathbb{B}_I^u \mathbf{u}_I \quad , \qquad \nabla\varphi = \sum_{I=1}^{m} \mathbb{B}_I^\varphi \varphi_I \ ,$$

The total strain displacement field and phase-field in an element is given by vectors

$$\mathbb{B}_I^u = \begin{bmatrix} N_{I,x} & amp; 0 \\ 0 & amp; N_{I,y} \\ 0 & amp; 0 \\ N_{I,y} & amp; N_{I,x} \end{bmatrix} , \ \mathbb{B}_I^\varphi = \begin{bmatrix} N_{I,x} \\ N_{I,y} \end{bmatrix} ,$$

The third row of $\mathbb{B}_I^u$, consisting of zeros, is required by the plane strain condition. A review of the work of Msekh[40] and starting with the numerical solution obtained external force is:

$$35 \quad \mathbf{F}^{\mathbf{u}}_{\mathrm{I\ ext}} = \int_\Omega \mathbf{N}_I^{\mathrm{uT}} \mathbf{b} + \int_{\partial\Omega} \mathbf{N}_I^{\mathrm{uT}} \mathbf{h} \ ,$$

And the internal forces are obtained from

$$36 \quad \mathbf{F}^{\mathbf{u}}_{\mathrm{I\ int}} = \int_\Omega g\left(\varphi, p\right) \mathbb{B}_I^{\mathbf{u}T} \sigma d\Omega \ ,$$

So that the discrete equations corresponding to stress equilibrium may be expressed as via the following residual:

$$37 \quad \mathbf{r}_I^{\mathbf{u}} = \mathbf{F}^{\mathbf{u}}_{\mathrm{I\ int}} - \mathbf{F}^{\mathbf{u}}_{\mathrm{I\ ext}} = \int_\Omega g\left(\varphi, p\right) \mathbb{B}_I^{\mathbf{u}T} \sigma d\Omega - \int_\Omega \mathbf{N}_I^{\mathrm{uT}} \mathbf{b} + \int_{\partial\Omega} \mathbf{N}_I^{\mathrm{uT}} \mathbf{h} \ ,$$

On the other hand, the residual corresponding to the evolution of the phase-field is given by

$$38 \quad \mathbf{r}_I^{\varphi} = \sum_{I=1}^{m} \int_\Omega \mathcal{G}_c \updownarrow B_I^{\varphi\mathrm{T}} \nabla\varphi + \left[\frac{\mathcal{G}_c}{\updownarrow} + 2\psi\left(\varepsilon\right)\right] N_I^\varphi \varphi d\Omega - \int_\Omega 2 N_I^\varphi \psi\left(\varepsilon\right) d\Omega \ ,$$

We seek the solution for which the$\mathbf{r}_I^{\mathbf{u}} = \mathbf{0}$ and$\mathbf{r}_I^{\varphi} = \mathbf{0}$. Due to the nonlinear nature of the residuals with respect to $\mathbf{u}$ and φ, we employ an incremental-iterative strategy utilizing the Newton–Raphson approach in conjunction with a parametrization based on a fictitious time:

$$39 \quad \begin{Bmatrix} u \\ \varphi \end{Bmatrix}_{t+t} = \begin{Bmatrix} u \\ \varphi \end{Bmatrix}_t - \begin{bmatrix} \mathbb{K}^{\mathrm{uu}} & amp; \mathbb{K}^{u\varphi} \\ \mathbb{K}^{\varphi u} & amp; \mathbb{K}^{\varphi\varphi} \end{bmatrix}_t^{-1} \begin{Bmatrix} \mathbf{r}^{\mathbf{u}} \\ \mathbf{r}^{\varphi} \end{Bmatrix}_t ,$$

In which

$$\mathbb{K}^{\mathrm{uu}} = \frac{\partial \mathbf{r}^{\mathbf{u}}}{\partial u} = \int_{\Omega} g\left(\varphi, p\right) \mathbb{B}^{\mathbf{u}T} \mathbf{C} \mathbb{B}^{\mathbf{u}} d\Omega \ ,$$

$$\mathbb{K}^{\mathbf{u}\varphi} = \frac{\partial \mathbf{r}^{\mathbf{u}}}{\partial \varphi} = \int_{\Omega} g_{,\varphi}\left(\varphi, p\right) \mathbb{B}^{\mathbf{u}T} \sigma N^{T} d\Omega \ ,$$

$$\mathbb{K}^{\varphi\mathbf{u}} = \frac{\partial \mathbf{r}^{\varphi}}{\partial u} = \int_{\Omega} g_{,\varphi}\left(\varphi, p\right) N \sigma^{T} \mathbb{B}^{\mathbf{u}} d\Omega \ ,$$

$$\mathbb{K}^{\varphi\varphi} = \frac{\partial \mathbf{r}^{\varphi}}{\partial \varphi} \int_{\Omega} \mathcal{G}_c \updownarrow \mathbb{B}^{\varphi \mathrm{T}} \mathbb{B}^{\varphi} + \left[\frac{\mathcal{G}_c}{\updownarrow} + 2\psi^{e}\left(\varepsilon\right)\right] N N^{T} d\Omega \ ,$$

The practical details in the Assembling algorithm for matrices are discussed in Appendix A.

4. Algorithmic aspects

4.1 Staggered solution strategy

Based on the algorithmic paradigm by Miehe *et al* [8], the proposed equations solved the weak formulations of mentioned equations in section 2 using a staggered strategy(Appendix C)The collection of equations as a result of the finite element model is nonlinear in order that one has to utilize to incremental-iterative schemes for calculating the solution. The proposed model has been realized into application within the software ABAQUS in order to take advantage of its built-in nonlinear solver using the Newton–Raphson algorithm along with automatic time-step control technique.

Respecting to the phase-field model for brittle fracture in two-dimensional and its extension to ductile one, an 8-node quadrilateral element is defined with 3 DOF per node, which are respectively u_x, u_y and φ. These parameters were implemented into an interface element in the UEL user subroutine in the finite element code ABAQUS.

The subroutine is the readout for every element and gets the nodal values of the element as input. The Abaqus user subroutine employs the displacement increments to compute incremental strain and called user subroutine UMAT to achieve the stress increment and the material jacobian. The latter is needed to matrix A. Implemented formulations of the stiffness matrix and force vector in section 2 of the element calculate to matrix A and the vector F and saves them in the arrays AMATRX and RHS as subroutine's built-in parameters. In another word, Abaqus collects contributions from all elements, forms global matrix A and vector F and finds a correction vector

$\begin{Bmatrix} u \\ \varphi \end{Bmatrix}_{t+t}$via solving Eq. (39).

4.2 Time integration

To develop accurate, efficient, and stable integration rules for integrating the set of the constitutive (differential) equations of the proposed elastoplastic model in section 2, explicit numerical integration methods were considered. To keep the presentation simple, the integration strategy has been presented briefly. The generalization of these integration techniques for a set of PDEs is forthright and presented afterward.

$$\varepsilon^{\varepsilon}_{\mathbf{n+1}} = \varepsilon^{\varepsilon}_{\mathbf{n}} + \lambda \sqrt{\tfrac{3}{2}} n_{n+1} \quad , \qquad \alpha_{n+1} = \alpha_n + \lambda \ ,$$

To solve the Eq.(41), extension of the return mapping algorithm made taking into account a special treatment of the phase-field development.[41,42]

Dependent on the small elastic strain tensor,$\varepsilon^{\mathbf{e}}$, plastic strain tensor,$\varepsilon^{\mathbf{p}}$, and the internal strain like scalar hardening variable, α, the problem of the increment calculation of $\varepsilon^{\mathbf{e}}$and $\varepsilon^{\mathbf{p}}$typically solved by an operator split into an elastic predictor and plastic corrector.[43,45] The calculation of the trial elastic state $(\ )^{\mathrm{tr}}$ according to theJ_2-plasticity model with linear isotropic hardening and based on freezing the plastic flow at the time $t_{\ n+1}$ is given by,

$$\sigma_{n+1}^{\mathrm{tr}} = 2\gamma\mu\varepsilon_{n+1}^{e,\ \mathrm{tr}} \quad , \qquad f_{n+1}^{\mathrm{tr}}\left(\sigma,\alpha,\varphi,p\right) = \sqrt{3J_2\sigma_{n+1}^{\mathrm{tr}}} - \left(\sigma_y + h\alpha\right) \leq 0,$$

The usual yield function proved in Eq. (42) does not produce precise physical response while linked with the phase-field model for crack growth. In the process of material failure, the damaged elastic reaction pulls the stress back within the yield surface and any further deformation up to complete failure is purely elastic.[27] That is opposite to what is noticed physically for ductile materials where the deformation is controlled by plastic strain. To compensate for this behavior, plastic degradation function should take place in the yield surface. [46]

$$\sqrt{3J_2\sigma_{n+1}^{\mathrm{tr}}} - \left(\sigma_y + h\alpha\right) - h\lambda - g_p 3\mu\lambda = 0 \ ,$$

Otherwise speaking, g_p is the plastic degradation function. The plastic degradation function is resembling the elastic degradation function and provides a mechanism for driving crack growth by the development of plastic strains. As a result, the case with $g_p = 1$, there is no plastic softening.

5. Numerical examples

The performance of the applied model is tested with the aid of several examples of the potential to capture representative aspects of fracture processes in ductile materials inside the proposed method, starting with the simplest one-the homogeneous plate subjected to pure tensile loading.

Table . Material Properties

Properties Materials	*Material I*	*Material II*	*Material III*	*Material IV*	*Material V*
Bulk modulus	71,660 MPa	1,36,500 MPa	1,36,500 MPa	71,660 MPa	2,20,000 MPa
Yield stress	345 MPa	443 MPa	443 MPa	345 MPa	864 MPa
Hardening modulus	250 MPa	300 MPa	1690 MPa	2,500 MPa	850 MPa
Critical fracture Energy	9.31 MPa mm	20.9 MPa mm	20.9 MPa mm	9.31 MPa mm	9.31 MPa mm

Initially, the I-shape specimen is examined to show the accuracy of the crack pattern, the role of a q parameter, and the load-carrying capacity of the specimen. In the next step, the single edge tension test is used to evaluate the effect of the loading angle and role of the n parameter in combination with the proposed q parameter.

Finally, double notched specimens and a compact tension specimen were studied to evaluate the robustness of the proposed model. In this process, the crack trajectory, role of length scale, and strain threshold on the load-displacement behavior were tested. All numerical computations are performed within the finite element framework using fully integrated 8-node quadrilateral elements and assuming plain strain conditions, with the material properties as mentioned before. Displacement controlled conditions are always assumed. Moreover, all of the simulations are performed on an Intel® Xeon® CPU E5-2690 v4 @ 2.60 GHz with 24 GB RAM memory. The calibration parameters are described as follows.

Table . Calibration Parameters

Specimens Simulation parameters	$\varepsilon^{\mathbf{P}}_{\mathrm{eq,crit}}$	**q**	**n**	**m**	↕ *(mm)*
I-shaped specimen	15%	0.1	1.5	3	1
Single-edge notched specimen (Tension)	4%	0.1	1.5 & 2	3	0.01
Single-edge notched specimen (Shear)	10%	1	1.5 & 2	3	0.1
Asymmetrically notched specimen	4%	0.3	2	3	0.4
Double notched specimen	5% − 16%	0.1	2	3	0.1
Compact tension (CT) specimen	5%	1	2	3	0.1 & 0.2

5.1 A homogeneous plate subjected to tension

A two-dimensional homogeneous plate with dimensions of1 × 1 mm is discretized by one element. The computation is performed by $u = 1$ mm for 1000 steps. The following material properties are chosen: The Young's modulus $E = 71$ GPa, Poisson's ratio $\vartheta = 0.3$ and critical fracture energy density$\mathcal{G}_c = 9.310$ kN/mm. As the characteristic size of the element is 1 mm, the length scale parameter is set to $l = 2$ mm.

Setting the crack surface gradient to zero, corresponding to the homogeneous case ($\nabla\varphi = 0$). Thus, the axial stress can be calculated as$\sigma(\mathbf{u},\varphi) = g(\varphi)\frac{\partial\psi_e(\varepsilon)}{\partial\varepsilon} = g(\varphi)\,\mathbb{C}:\varepsilon$, with $\psi_e(\varepsilon) = {\psi_e}^{+}(\varepsilon)$ and${\psi_e}^{-}(\varepsilon) = 0$ because of the pure tension loading. Dimension and boundary conditions for numerical examples are listed in Table 3.

Table . Dimension and boundary conditions for all of the tested specimens

I-shaped specimen. Geometry and boundary conditions.[15] Dimensions in mm
Single-edge notched tension test. a) Geometry and boundary conditions. [49] Dimensions in mm. b) Finite element models
Single-edge notched shear test. a) Geometry and boundary conditions. [49] Dimensions in mm. b) Finite element models a
Asymmetrically notched specimen. a) Geometry and boundary conditions.[49] Dimensions in mm. b) Finite element mode
Double notched specimen tension test. [54] a) Geometry and boundary conditions. Dimensions in mm. b) Finite element r
CT specimen tension test [49]. Dimensions in mm. a) Geometry and boundary conditions. Dimensions in mm, b) Finite el

5.2 I-shaped specimen

To compare the accuracy of the proposed model on the prediction of the crack path and load-displacement behavior, a tensile test on the I-shaped specimen with the geometric properties and boundary conditions shown in Table 3-I have been analyzed. The bottom edge is restrained vertically and displaced horizontally, whereas the left edge is fixed. The displacement boundary condition is applied to the right edge. The material parameters are those of Material I in Table 1. A uniform mesh with 12230 quadrilateral elements is used.

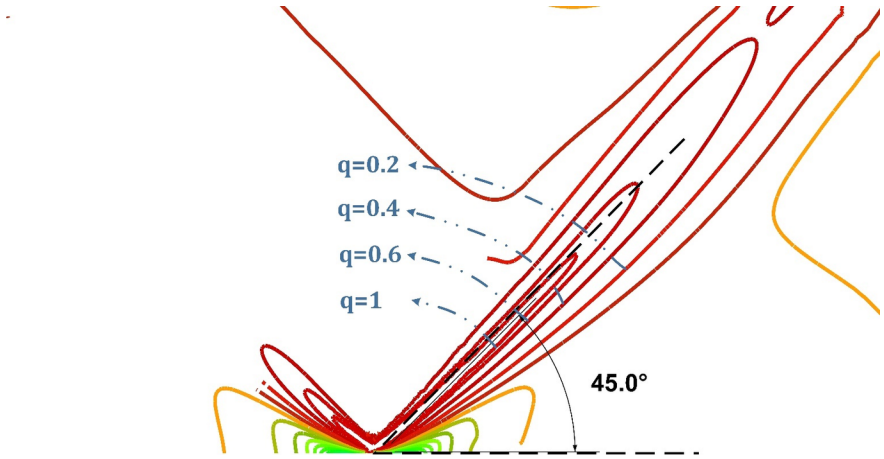

Fig.**1** Line plot of I-shaped specimen and demonstration of the effect of **q**parameter in the completeness of failure. (blue dashes), crack propagation direction (black dashes)

From Fig.1, it can be seen that the variation of q parameter affects the stage of fracture process in terms of the crack path. In addition, the q parameter controls the stability of the crack propagation. For I-shaped specimens in plane-strain conditions, experimental data indicates that the crack forms in the middle of the specimen with an inclination of about ± 45 in relation to the main stress direction.[47]

Miehe *et al* [8] suggested using the viscosity parameter to overcome the instability of crack growth. In the proposed model in this study, this is done by reducing the computational complexity by introducing the q parameter. The results of investigations on the q parameter have shown that the use of high values for this parameter leads to divergence of analysis. As such for q=1, the crack grows to the middle of the sample and then diverges. While for q=0.2, the crack growth is complete and the results agree very well with other similar works. The corresponding load-displacement curve is shown in Fig.2. The sudden drop in the curve is due to the onset of crack phase-field localization.

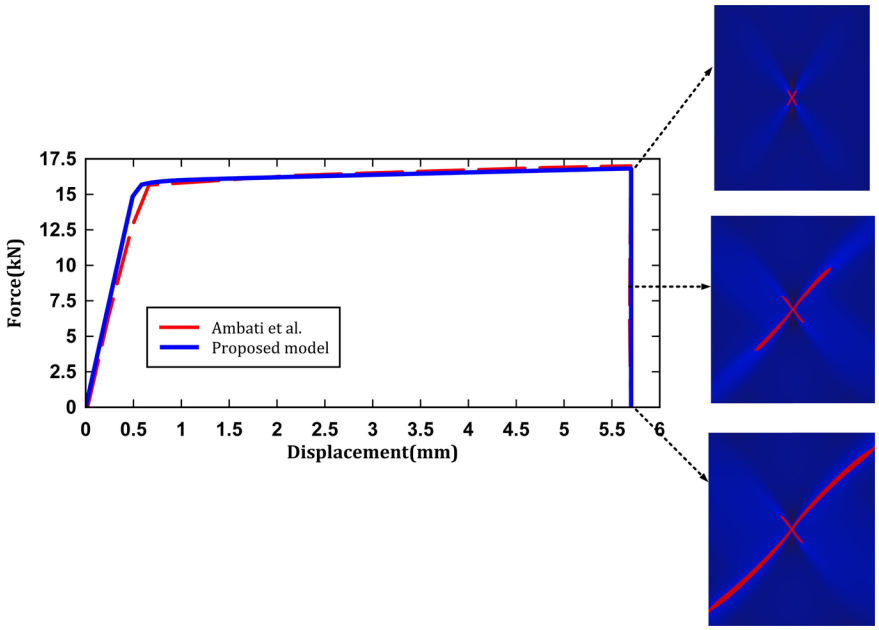

Fig.2 The load-displacement curve for the I-shaped specimen. Contour plots of the fracture phase field at various stages

5.3 Single-edge notched specimen

This is the most common benchmark test used in the verification of the phase-field fracture models. The single-edge notched test is investigated in detail, both experimentally and numerically.[48-51] The same investigation performed to compare predictions of the proposed phase-field model with the aforementioned results. Firstly, the specimen is subjected to the tensile load, where the effect of n parameter is considered. Afterward, the specimen is subjected to the shear load, where the proposed model is tested with the two different values of the n. Loading is applied by $\Delta u = \ 10e-3$ mm for 1000 steps.

5.3.1 Single-edge notched tension test

The boundary conditions used in this example are shown in Table 3-II. The specimen domain is discretized by 10455 finite elements.

Fig.3 depicts the crack phase-field at several stages. In the illustrated Single-edge notched tension test the crack propagates horizontally. A phenomenon that is observed in the simulation is that the phase-field evolution takes place mainly in front of the crack tip which results in stable crack propagation. The crack pattern is in agreement with both the works of Miehe *et al* . and Ambati *et al* .[52,48,15] The force-displacement curves in Fig.4 exhibiting ductile behavior.

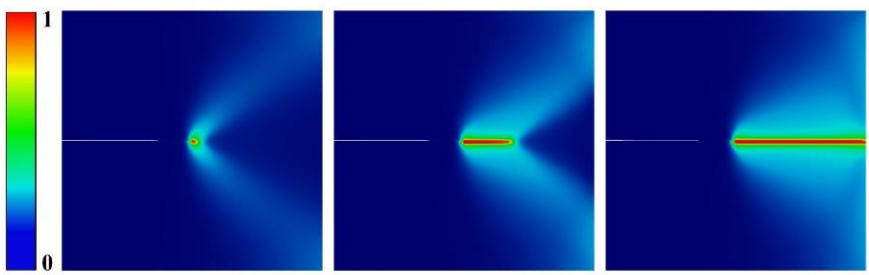

Fig. Single-edge notched tension test. crack phase-field contour plot for **n= 1.5**and **n= 1.8** (quite similar) in various stages

In Fig.4, for smaller values of n , the curve becomes more unstable at the end and drops with more steeply, and failure occurs suddenly. In this situation, the cracks may deviate from the straight path and grow in the wrong direction. Hence, the use of larger values of$n$ can lead to more accurate results.

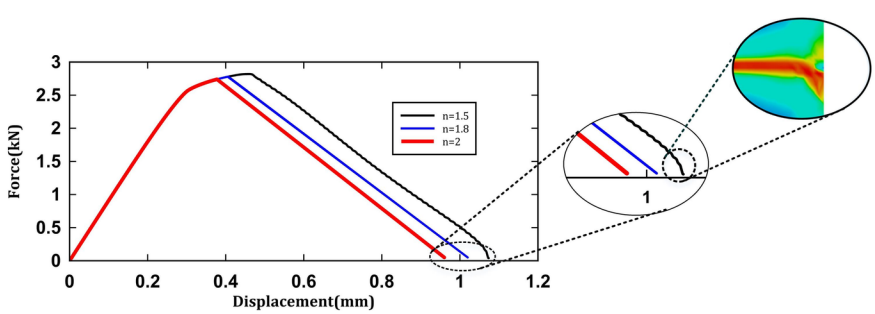

Fig. The load-displacement curve for a single-edge notched specimen for different values of n

5.3.2 Single-edge notched shear test

The boundary conditions are presented in Table 3-III for load applying direction of 45. The mesh consists of 4056 finite elements and is refined in the expected crack propagation area. Fig.5 shows the crack pattern solution for $n = 2$ and $n = 1.5$.

Fig.6 shows the computed load-displacement curve and variation of the reaction force over the loading history. As is shown, the normal ductile behavior proceeds until the crack initiates. However, the crack propagation is so brutal. The n value also influence the load carrying capacity of the specimen. The crack starts to propagate at a higher applied displacement as the value of n decreases, leading to a higher load carrying capacity of the specimen. This numerical example shows that large n values lead to brittle fracture while small $n$values result in ductile fracture. The proposed phase-field model is capable of simulating both brittle fracture and ductile fracture as well as the ductile-brittle transition if n is set to be a function of field variables such as q parameter.

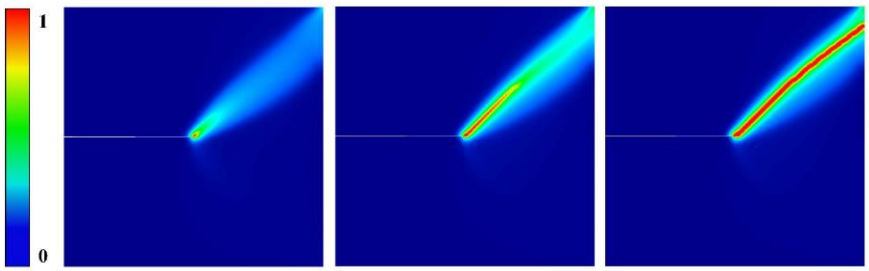

Fig. Single-edge notched shear test. crack phase-field contour plot for **n= 1.5**and **n= 2** (quite similar) in various stages

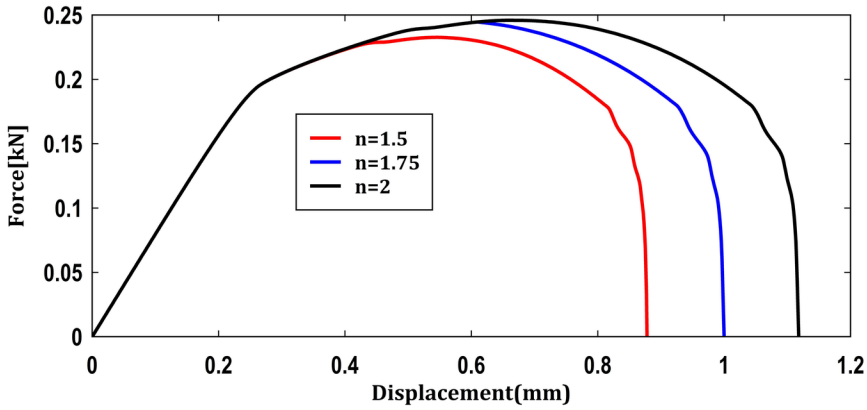

Fig. The load-displacement curve for a single-edge notched specimen for different values of n

5.5 Asymmetrically notched specimen

The asymmetrically notched specimen illustrated in Table 3-IV. The top edge is restrained horizontally and displaced vertically, whereas the bottom edge is fixed. The material parameters are those of Material IV in Table 1. The spatial discretization of the model comprises 4857 quadrilateral elements, with refinement in the central region between the notches where the crack is expected to form.

The evolution of the crack phase-fields is provided in Fig.7 for the proposed model. The developed model is able to predict crack initiation at the notches and take the right pattern between them. The initial cracks propagate within the plastic strain localization band and eventually merge leading to complete failure.

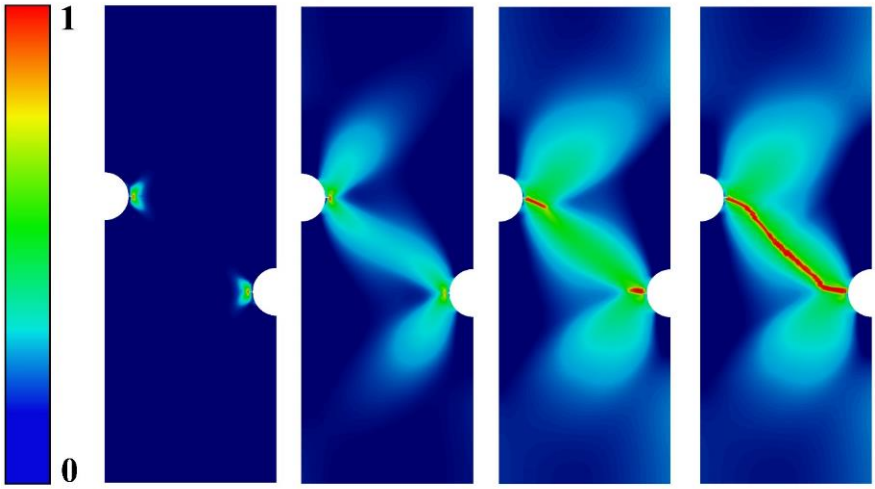

Fig. Asymmetrically notched specimen crack phase-field contour plot in various stages

The effect of the q parameter on results in terms of crack path is evaluated respectively in Fig.8. The Figure compares the crack path for the four cases. For $q = 1$, cracks initiate at the two notches and don't propagate toward the opposite side of the specimen. For $q = 0.8$ and $q = 0.5$, cracks initiate at the two notches and propagate until the middle of the specimen. The two cracks do not merge. For $q = 0.2$, cracks initiate and merge together, Fig.7.

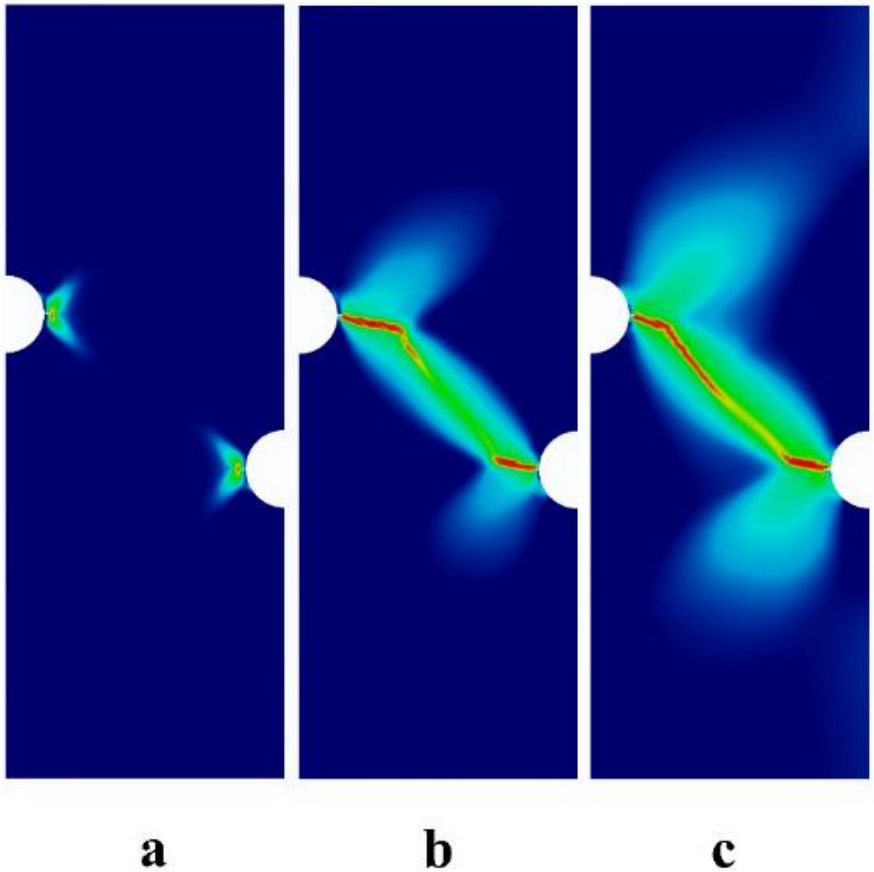

Fig.8 The effect of **q** parameter on the stability of crack propagation a) **q= 1** , b) **q= 0.8** , c)**q= 0.5**

The global aspect of the load-displacement curve is similar to that obtained with the previous investigations.[15,53]However, it should be noted that the general fracture process is quite different for the highest values of the hardening module. From the force-displacement curve, unlike Ambati *et al* , the initiation of the failure in the present material is not quite abrupt, Fig.9.

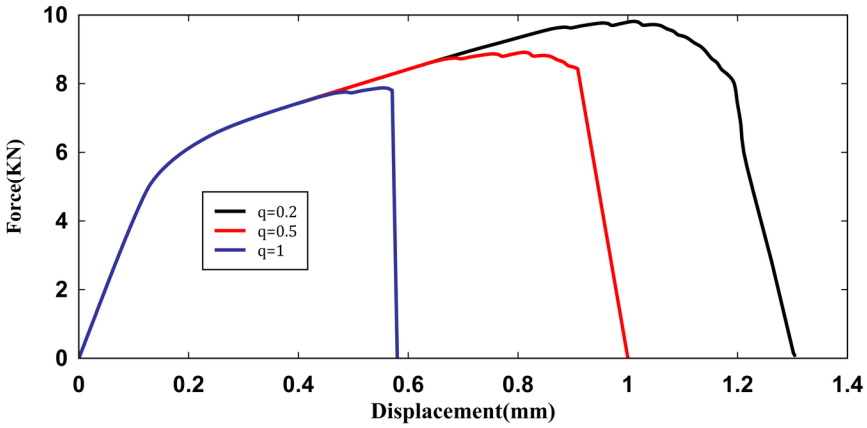

Fig. The load-displacement curve for asymmetrically notched specimen

5.4 Double notched specimen

A benchmark simulation has been performed in order to assess the robustness of the computations for different critical equivalent plastic strain. Motivated by the blanking process, a problem geometry with two asymmetrically placed rounded notches is used for this purpose.[54] The geometry and boundary conditions are given in Table 3-V. Vertical displacements are imposed on the top and left boundaries, while horizontal displacements have been prevented. The bottom and right boundaries are remained fixed. The material parameters are those of Material III in Table 1. The adopted discretization contains 13240 quadrilateral elements with mesh refinement in the expected crack propagation region.

In this illustrative example, the damage fields aren't quite smooth. The tensile loading causes the development of a plastic shear band between the two notches and gives rise to damage initiation at the notches. In the context of ductile fracture, the same problem has been addressed using a non-local damage model for the initial continuum damage phase, followed by a discontinuous crack propagation phase predicted through a remeshing strategy.[54] Results showed the development of a plastic shear band diagonally across the specimen, which in turn results in a curved crack trajectory which initiates at both the notches and propagates towards the center of the specimen where the two crack branches merge, Fig.10. It is worth noting that, with the increasing critical plastic strain, secondary cracks initiate at the surface of the top and bottom boundaries and start to propagate to the other side.

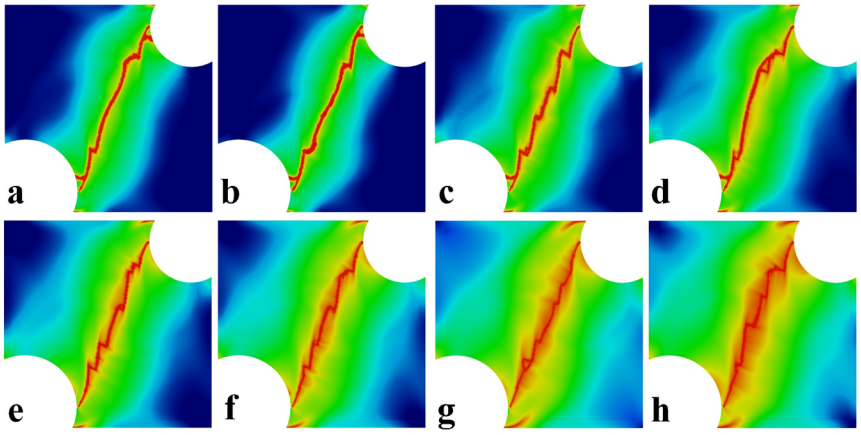

Fig. Crack trajectory for double notched specimen, a)$\varepsilon^{\mathbf{p}}_{\mathrm{eq,crit}}=\mathbf{5}\%$, b)$\varepsilon^{\mathbf{p}}_{\mathrm{eq,crit}}=\mathbf{6}\%$, c)$\varepsilon^{\mathbf{p}}_{\mathrm{eq,crit}}=\mathbf{8}\%$, d)$\varepsilon^{\mathbf{p}}_{\mathrm{eq,crit}}=\mathbf{9}\%$, e)$\varepsilon^{\mathbf{p}}_{\mathrm{eq,crit}}=\mathbf{10}\%$, f)$\varepsilon^{\mathbf{p}}_{\mathrm{eq,crit}}=\mathbf{12}\%$, g)$\varepsilon^{\mathbf{p}}_{\mathrm{eq,crit}}=\mathbf{14}\%$, h)$\varepsilon^{\mathbf{p}}_{\mathrm{eq,crit}}=\mathbf{16}\%$

Fig.11 shows the effect of critical plastic strain changes on the sample failure behavior. As can be seen in this figure, as the critical strain increases, the fracture initiation in the specimens is delayed and more force is required for the fracture. This result is consistent with the findings of the related literature.[15]

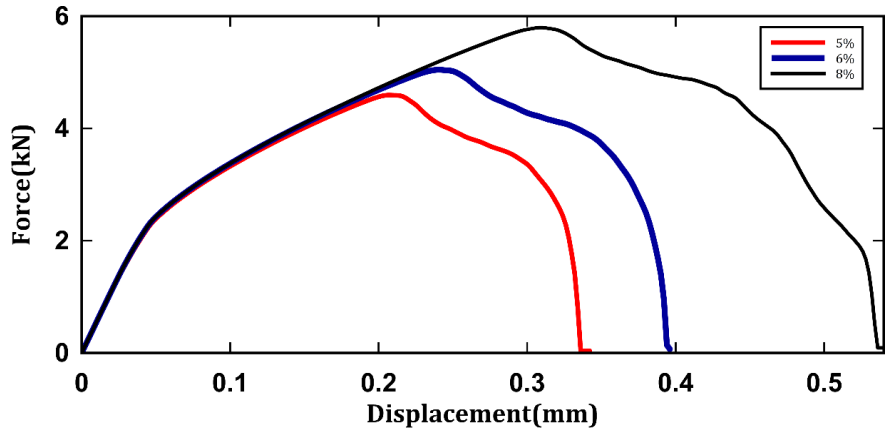

Fig. The influence of critical plastic strain on the load-displacement curve for double notched specimen

5.7 Compact tension (CT) specimen

Finally, the crack initiation and propagation for a CT specimen have been investigated. The geometry and boundary conditions are shown in Table 3-VI. The specimen contains a horizontal notch at its mid-height, and load is applied by a top pin which is displaced vertically, whereas the lower pin is fixed.

The material parameters are those of Material II in Table 1. The mesh comprises 14722 quadrilateral elements with refinement in the areas where the crack is expected to form. In this test, the q parameter does not significantly influence the crack path, the experimentally observed crack pattern being well captured for both $q = 1$ and$q = 0.5$.

The crack pattern results are shown in Fig.13. It can be observed a horizontal crack propagates inward from the notch tip. The phase-field failure simulation based on the proposed model indicates that a length scale of the specimen shows slight differences in the load-displacement curve. As is well known from the curve, the small length scale leads to more fracture-resistant than the large ones.

Fig.12 shows the measured load vs. crack extension behavior for CT specimens evaluated in this study. The general shape of these curves consists of a stable crack growth region characterized by increasing load during crack extension followed by an unstable crack growth region characterized by decreasing load during crack extension. The maximum fracture load for each test defines the transition from stable to unstable crack extension. Finally, the rather smooth drops in loading at the initiation of fracture for the cases that ignore the material weakening.

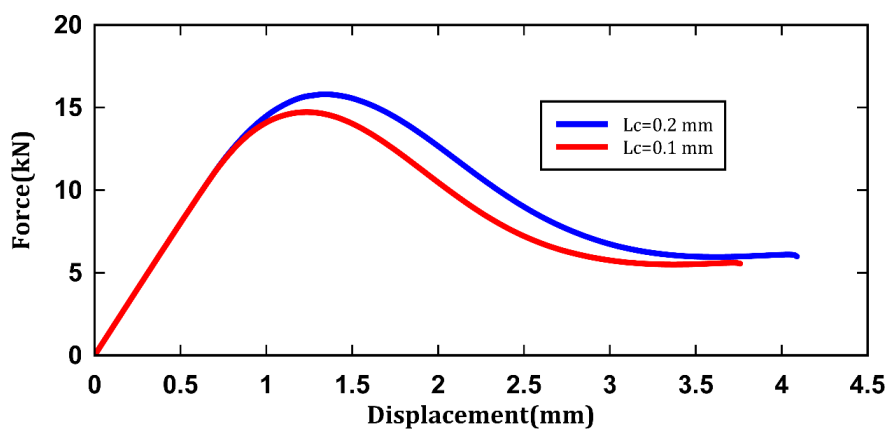

Fig. The load-displacement curve for CT specimen

The qualitative agreement between the computational and experimental crack pattern is excellent. Additionally, the shape of the curves from models considering the material weakening agrees well with the experimental curves. [15, 47,55]

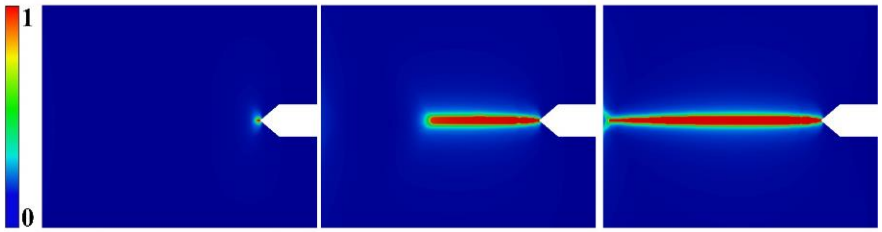

Fig. CT specimen tension test. The crack phase-field contour plot is shown in various stages

6. Conclusion

In this study, the phase-field model for ductile fracture proposed in Ambati[15] has been investigated in more detail, and its predictions have been compared with literature. The results obtained from the simulations are in good agreement with the previous investigations results. In particular, this study showed that the proposed model can capture the experimentally observed sequence of elastoplastic deformation and fracture phenomena in purposed specimens. Moreover, simulation precisely determined the impact of the critical plastic strain, length scale, and proposed parameters on the force-displacement response in the presence of the ductile behavior. The results also showed that not only crack patterns but also load-displacement curves aspects of the behavior could be accurately captured.

Appendix

Appendix A: Assembly algorithm for matrices

An algorithm of the assembly of the global stiffness matrix$\mathbb{K}$ from contributions of element stiffness matrices k can be expressed by the following pseudo-code:

n = number of degrees of freedom per element$N$ = total number of degrees of freedom in the domain$E$ = number of elements$C[E,\ n]$ = connectivity array$k[n,\ n]$ = element stiffness matrix$\mathbb{K}[N,\ N]$ = global stiffness matrix

do $i\ =\ 1,\ N$

do $j\ =\ 1,\ N$

$\mathbb{K}\ [i,\ j]\ =\ 0$

end do

end do

do $e\ =\ 1,\ E$

generate k

do $i\ =\ 1,\ n$

do $j\ =\ 1,\ n$

$\mathbb{K}\,[C[e,\ i],\ C[e,\ j]]\ =\ \mathbb{K}\,[C[e,\ i];\ C[e,\ j]]\ +\ k[i,\ j]$

end do

end do

end do

Here for simplicity, element matrices are assembled fully in the full square global matrix. Since the global stiffness matrix is symmetric and sparse, these facts are used to economize space and time in actual finite element codes.[56]

Appendix B: Detailed explanation of single element (*inp file)

This part demonstrates a practical single element example, which can be used to generate any model in ABAQUS/Standard with the implemented fracture model. The problem is a simple element subjected to uniaxial tension. The present *inp file demonstrates an element with eight nodes, in 2D, with material properties and twenty status variables. From this point, the displacement, boundaries and the analysis are defined usually as it is done in a normal input file. Moreover, putting a visualization command in the ASSEMBLY section pointing to the UMAT elements for post-processing purposes. [57],[40]

```
*Heading
*Preprint, echo=NO, model=NO, history=NO, contact=NO
********************************
*NODE
1, 0.0,0.0
2, 1.0,0.0
3, 1.0,1.0
4, 0.0,1.0
5, 0.5,0.0
6, 1.0,0.5
7, 0.5,1.0
8, 0.0,0.5
*NSET, NSET=BOTTOM
1,2,5
*NSET, NSET=TOP
3,4,7
*NSET, NSET=MIDDLE
6,8
*NSET, NSET=EDGES
3,4,6,8
*NSET, NSET=ALLNODES
BOTTOM, TOP, MIDDLE
```

```
*AMPLITUDE, NAME=DIS
0.000,0.000,1.0,1.0
********************************
*USER ELEMENT, NODES=8, TYPE=U1, PROPERTIES=6, COORDINATES=2, VARIABLES=200
1,2
1,12
*ELEMENT, TYPE=U1, ELSET=TODOS
1,1,2,3,4,5,6,7,8
********************************
*UEL PROPERTY, ELSET=TODOS
71660,0.3,345.0,0.0,407.5,0.25
********************************
*ELEMENT, TYPE=CPE8, ELSET=dummy
2 ,1,2,3,4,5,6,7,8
********************************
*Solid Section, elset =dummy, material=dummy
1.0
*Material, name=dummy
*Depvar
20,
*User Material, constants=2
1.0e-11,0.3
********************************
*STEP, INC=10000000, EXTRAPOLATION=NO, nlgeom=NO
*STATIC, DIRECT=NO STOP
1.0E-3,1.0,1.0E-7,1.0E-3
********************************
*BOUNDARY
BOTTOM, ENCASTRE
*BOUNDARY, TYPE=DISPLACEMENT
TOP,2,2,0.1
********************************
*Restart, write, frequency=0
*Output, field
```

*element output, elset=dummy

Sdv21

*Node Output

RF, U

*Output, history, variable=PRESELECT

*Node Output, nset =top

RF2

*End Step

Appendix C: Umat &UEL Algorithmic Paradigm

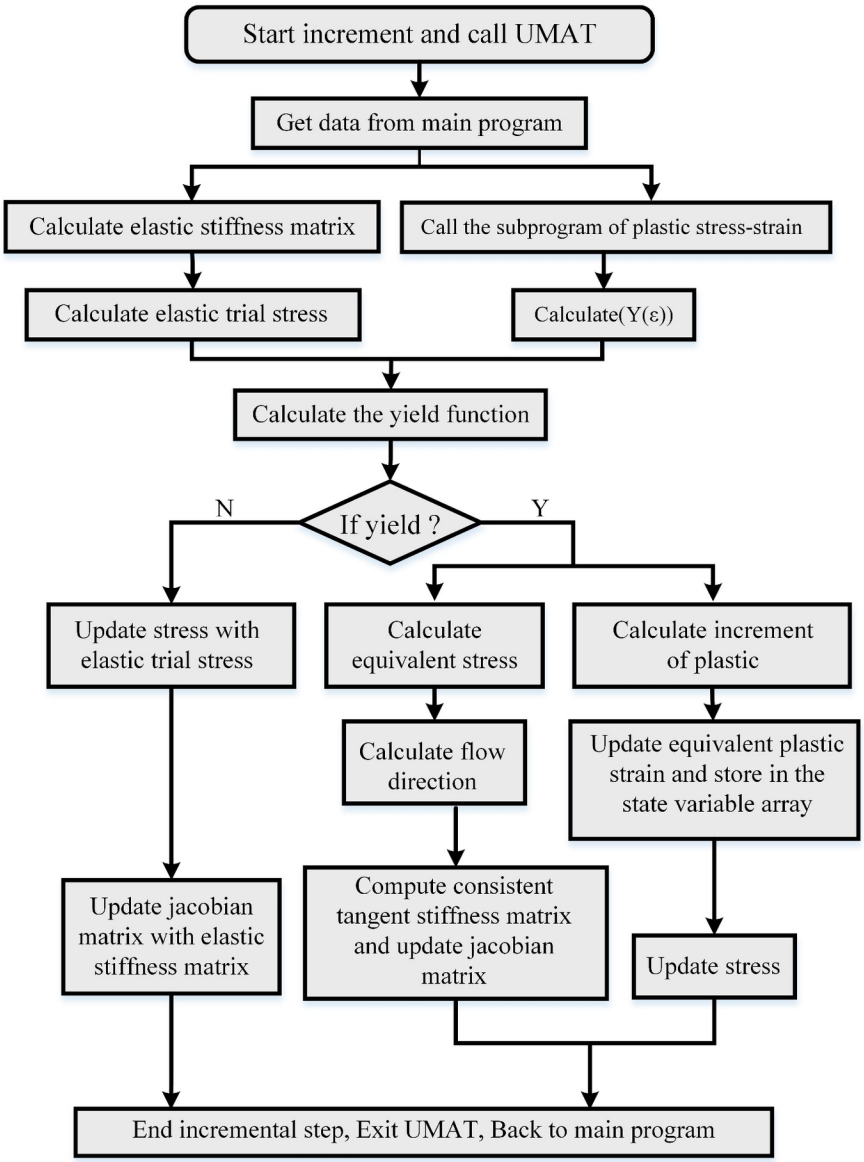

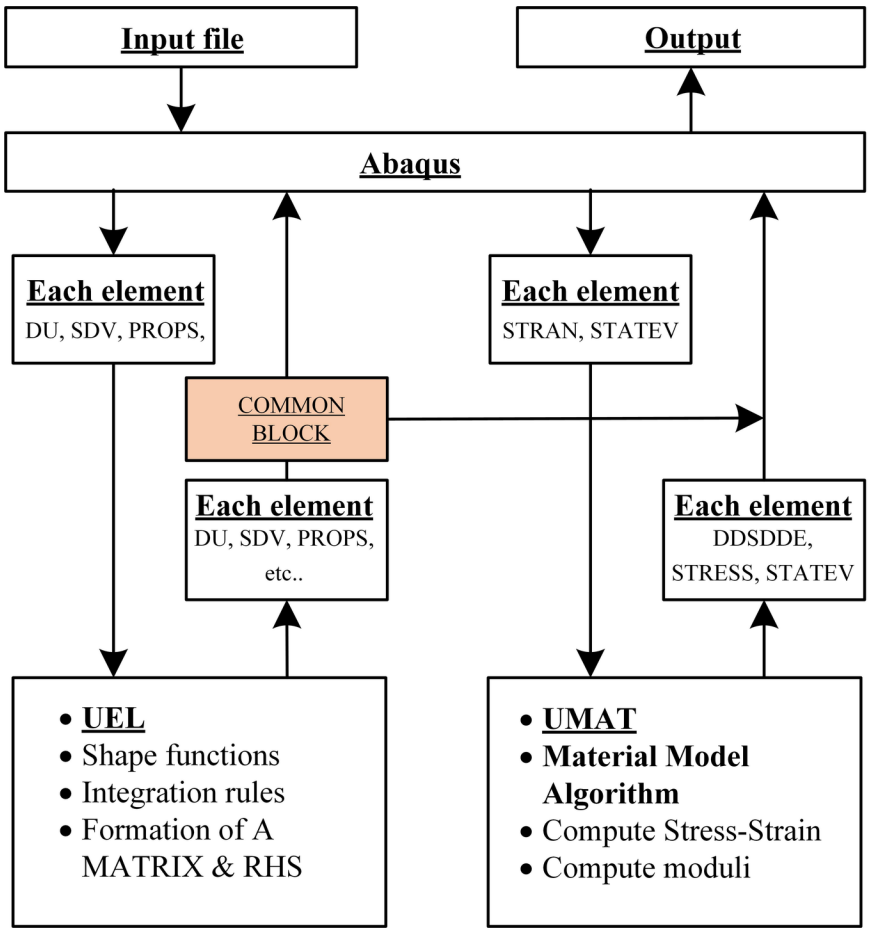

Data Availability' statement

The data required to reproduce these findings are available from the corresponding authors upon reasonable request.

Reference

1. Besson J. Continuum models of ductile fracture: A review.*International Journal of Damage Mechanics* . 2010;19(1):3–52.

2. Griffith AA. The Phenomena of Rupture and Flow in Solids.*Philosophical Transactions of the Royal Society A: Mathematical, Physical and Engineering Sciences* . 1921;221(582–593):163–98.

3. Kuhn C, Müller R. A continuum phase field model for fracture.*Engineering Fracture Mechanics* . 2010;77(18):3625–34.

4. Hakim V, Karma A. Laws of crack motion and phase-field models of fracture. *Journal of the Mechanics and Physics of Solids* . 2009;57(2):342–68.

5. Francfort GA, Marigo JJ. Revisiting brittle fracture as an energy minimization problem. *Journal of the Mechanics and Physics of Solids* . 1998;46(8):1319–42.

6. Mumford D, Shah J. Optimal approximations by piecewise smooth functions and associated variational problems. *Communications on Pure and Applied Mathematics* . 1989;42(5):577–685.

7. Bourdin B, Francfort GA, Marigo JJ. Numerical experiments in revisited brittle fracture. *Journal of the Mechanics and Physics of Solids* . 2000;48(4):797–826.

8. Miehe C, Hofacker M, Welschinger F. A phase field model for rate-independent crack propagation: Robust algorithmic implementation based on operator splits. *Computer Methods in Applied Mechanics and Engineering* . 2010;199(45–48):2765–78.

9. Miehe C, Welschinger F, Hofacker M. Thermodynamically consistent phase-field models of fracture: Variational principles and multi-field FE implementations. *International Journal for Numerical Methods in Engineering* . 2010;83(10):1273–311.

10. Larsen CJ. Models for dynamic fracture based on Griffith's criterion. *IUTAM Bookseries* . 2010;21:131–40.

11. LARSEN CJ, ORTNER C, SÜLI E. Existence of Solutions To a Regularized Model of Dynamic Fracture. *Mathematical Models and Methods in Applied Sciences* . 2010;20(07):1021–48.

12. Bourdin B, Larsen CJ, Richardson CL. A time-discrete model for dynamic fracture based on crack regularization. *International Journal of Fracture* . 2011;168(2):133–43.

13. Borden MJ, Verhoosel C V., Scott MA, Hughes TJR, Landis CM. A phase-field description of dynamic brittle fracture. *Computer Methods in Applied Mechanics and Engineering* . 2012;217–220:77–95.

14. Hofacker M, Miehe C. A phase field model of dynamic fracture: Robust field updates for the analysis of complex crack patterns.*International Journal for Numerical Methods in Engineering* . 2013;93(3):276–301.

15. Ambati M, Gerasimov T, De Lorenzis L. Phase-field modeling of ductile fracture. *Computational Mechanics* . 2015;55(5):1017–40.

16. Ambati M, Kruse R, De Lorenzis L. A phase-field model for ductile fracture at finite strains and its experimental verification.*Computational Mechanics* . 2016;57(1):149–67.

17. Miehe C, Hofacker M, Schänzel L-M, Aldakheel F. ScienceDirect Phase field modeling of fracture in multi-physics problems. Part II. Coupled brittle-to-ductile failure criteria and crack propagation in thermo-elastic–plastic solids. *Comput Methods Appl Mech Engrg* . 2014;

18. Miehe C, Aldakheel F, Raina A. Phase field modeling of ductile fracture at finite strains: A variational gradient-extended plasticity-damage theory. *International Journal of Plasticity* . 2016;84:1–32.

19. Broka SM, Dubois PE, Joucken KL. A structural deficiency of TCI syringes [6]. *Anesthesia and Analgesia* . 2000;90(4):1002–3.

20. Hofacker M, Miehe C. A Phase Field Model for Ductile to Brittle Failure Mode Transition. *Pamm* . 2012;12(1):173–4.

21. Miehe C, Teichtmeister S, Aldakheel F. Phase-field modelling of ductile fracture: A variational gradient-extended plasticity-damage theory and its micromorphic regularization. *Philosophical Transactions of the Royal Society A: Mathematical, Physical and Engineering Sciences* . 2016;374(2066).

22. Duda FP, Ciarbonetti A, Sánchez PJ, Huespe AE. A phase-field/gradient damage model for brittle fracture in elastic-plastic solids. *International Journal of Plasticity* . 2014;65:269–96.

23. Gerasimov T, De Lorenzis L. On penalization in variational phase-field models of brittle fracture. *Computer Methods in Applied Mechanics and Engineering* . 2019;354:990–1026.

24. Brach S, Tanné E, Bourdin B, Bhattacharya K. Phase-field study of crack nucleation and propagation in elastic–perfectly plastic bodies.*Computer Methods in Applied Mechanics and Engineering* . 2019;353:44–65.

25. Sargado JM, Keilegavlen E, Berre I, Nordbotten JM. High-accuracy phase-field models for brittle fracture based on a new family of degradation functions. *Journal of the Mechanics and Physics of Solids* . 2018;111:458–89.

26. Bourdin B, Francfort GA, Marigo JJ. The variational approach to fracture. *The Variational Approach to Fracture* . 2008;1–164.

27. Borden MJ, Hughes TJR, Landis CM, Anvari A, Lee IJ. Corrigendum to "A phase-field formulation for fracture in ductile materials: Finite deformation balance law derivation, plastic degradation, and stress triaxiality effects" [Comput. Methods Appl. Mech. Engrg. 312 (2016) 130–166](S0045782516311069)(10.1016. *Computer Methods in Applied Mechanics and Engineering* . 2017;324:712–3.

28. Amor H, Marigo JJ, Maurini C. Regularized formulation of the variational brittle fracture with unilateral contact: Numerical experiments. *Journal of the Mechanics and Physics of Solids* . 2009;57(8):1209–29.

29. Contrafatto L, Cuomo M. A framework of elastic-plastic damaging model for concrete under multiaxial stress states. *International Journal of Plasticity* . 2006;22(12):2272–300.

30. Comi C, Perego U. Fracture energy based bi-dissipative damage model for concrete. *International Journal of Solids and Structures* . 2001;38(36–37):6427–54.

31. Faria R, Oliver J, Cervera M. A strain-based plastic viscous-damage model for massive concrete structures. *International Journal of Solids and Structures* . 1998;35(14):1533–58.

32. Ambati M, Gerasimov T, De Lorenzis L. A review on phase-field models of brittle fracture and a new fast hybrid formulation.*Computational Mechanics* . 2014;55(2):383–405.

33. Larsen, CJ; O, C; S, E. Existence of Solutions To a Regularized Model of Dynamic Fracture. *Mathematical Models & Methods in Applied Sciences* . 2010;20(7):1021–48.

34. Schlüter A, Willenbücher A, Kuhn C, Müller R. Phase field approximation of dynamic brittle fracture. *Computational Mechanics* . 2014;54(5):1141–61.

35. Ambati M, Gerasimov T, De Lorenzis L. Phase-field modeling of ductile fracture. *Computational Mechanics* . 2015;55(5):1017–40.

36. Computational inelasticity. Vol. 37, Computers & Mathematics with Applications. 2003. 134 p.

37. Ambrosio L, Tortorelli VM. Approximation of functional depending on jumps by elliptic functional via t-convergence. *Communications on Pure and Applied Mathematics* . 1990;43(8):999–1036.

38. Development of Eight Node Isoparametric Quadrilateral (QUAD8) Elements in Java.

39. Function S. 18 18–1. :1–15.

40. Msekh MA, Sargado JM, Jamshidian M, Areias PM, Rabczuk T. Abaqus implementation of phase-field model for brittle fracture.*Computational Materials Science* . 2015;96(PB):472–84.

41. Eduardo A. de Souza Neto, Djordje Peric DRJO. Computational Methods for Plasticity: Theory and Applications.

42. PETRINIC FDAN. Introduction to Computational Plasticity.

43. Simo, J.C., Hughes TJR. Computational Inelasticity.

44. Simo J ˜C. Topics on the numerical analysis and simulation of plasticity. *Handbook of Numerical Analysis* . 1999;III.

45. Auricchio F, Taylor RL. Two material models for cyclic plasticity: Nonlinear kinematic hardening and generalized plasticity.*International Journal of Plasticity* . 1995;11(1):65–98.

46. Borden MJ, Hughes TJR, Landis CM, Anvari A, Lee IJ. A phase-field formulation for fracture in ductile materials: Finite deformation balance law derivation, plastic degradation, and stress triaxiality effects. *Computer Methods in Applied Mechanics and Engineering* . 2016;312:130–66.

47. Xue L, Xue Liang. Ductile fracture modeling: theory, experimental investigation and numerical verification. *PhD Thesis* . 2007;251.

48. Mediavilla J, Peerlings RHJ, Geers MGD. Discrete crack modelling of ductile fracture driven by non-local softening plasticity.*International Journal for Numerical Methods in Engineering* . 2006;66(4):661–88.

49. Mediavilla J, Peerlings RHJ, Geers MGD. A robust and consistent remeshing-transfer operator for ductile fracture simulations.*Computers and Structures* . 2006;84(8–9):604–23.

50. Amstutz BE, Sutton MA, Dawicke DS, Bonne M l. Effects of Mixed Mode I/II Loading and Grain Orientation on Crack Initiation and Stable Tearing in 2024-T3 Aluminum. *Fatigue and Fracture Mechanics* . 1997;27:105–25.

51. Hashin Z, Voloshin A. A Method to Produce Uniform Plane-stress States with Applications to Fiber-reinforced Materials. :141–6.

52. Tvergaard V, Needleman A. Analysis of the cup-cone fracture in a round tensile bar. *Acta Metallurgica* . 1984;32(1):157–69.

53. Rodriguez P, Ulloa J, Samaniego C, Samaniego E. A variational approach to the phase field modeling of brittle and ductile fracture.*International Journal of Mechanical Sciences* . 2018;144:502–17.

54. Mediavilla J, Peerlings RHJ, Geers MGD. A robust and consistent remeshing-transfer operator for ductile fracture simulations.*Computers and Structures* . 2006;84(8–9):604–23.

55. Mahmoud S, Lease K. The effect of specimen thickness on the experimental characterization of critical crack-tip-opening angle in 2024-T351 aluminum alloy. *Engineering Fracture Mechanics* . 2003;70(3–4):443–56.

56. Introduction to the finite element method. *Studies in Mathematics and its Applications* . 1978;4(C):36–109.

57. Molnar G, Gravouil A. 2D and 3D Abaqus implementation of a robust staggered phase-field solution for modeling brittle fracture.*Finite Elements in Analysis and Design* . 2017;130:27–38.

Hosted file

`Tables.docx` available at https://authorea.com/users/322843/articles/451775-fracture-investigation-of-the-ductile-materials-using-phase-field-model

Hosted file

`Figures for Fatigue & ....docx` available at https://authorea.com/users/322843/articles/451775-fracture-investigation-of-the-ductile-materials-using-phase-field-model